Index Modulation Based ISAC

Dingyou Ma, Tianyao Huang, Nir Shlezinger, Yimin Liu, and Yonina C. Eldar

Abstract Index modulation (IM) is a promising communications technique gaining growing interest due to its high energy and spectral efficiency. In addition to using conventional modulations, IM also embeds data bits into the indices of certain waveform parameters, such as the selection of active antennas and the sub-carriers. Recently, IM has been introduced to design ISAC systems by embedding the digital message into the combinations of waveform parameters. Through IM, the information is encapsulated in the combinations of waveform parameters as well as the symbol constellation, leading to an increase in data rates. For the radar subsystem, the randomization in the waveform parameters, such as carrier frequencies and antenna elements, enables to reduce the hardware complexity while has minimal influence to the radar resolution, which is attractive to many cost limited applications. In this chapter, we provide an overview of IM for ISAC. We begin by formulating the generic model of IM-based ISAC systems. Subsequently, some instances of existing IM-based ISAC systems are discussed using the generic model. In the next, the signal processing algorithms for both radar and communications systems are surveyed. The performance metrics of IM-based ISAC systems are discussed, and evaluated through simulation. Finally, concluding remarks and future challenges are provided.

D. Ma
School of Information and Communication Engineering, Beijing University of Posts and Telecommunications, Beijing, China
e-mail: dingyouma@bupt.edu.cn

T. Huang (✉) · Y. Liu
Department of Electronic Engineering, Tsinghua University, Beijing, China
e-mail: huangtianyao@tsinghua.edu.cn

Y. Liu
e-mail: yiminliu@tsinghua.edu.cn

N. Shlezinger
School of Electrical and Computer Engineering in Ben-Gurion University, Be'er-Sheva, Israel
e-mail: nirshl@bgu.ac.il

Y. C. Eldar
Department of Mathematics and Computer Science, Weizmann Institute of Science, Rehovot, Israel
e-mail: yonina.eldar@weizmann.ac.il

F. Liu et al. (eds.), *Integrated Sensing and Communications*,
https://doi.org/10.1007/978-981-99-2501-8_9

1 Introduction

Index modulation (IM) is an emerging communication technique for its advantages of high energy and power efficiency [2, 7, 12, 29]. In IM, the information is not only conveyed through traditional constellation symbols, but also embedded into the combinations of waveform parameters, such as the carrier frequencies, the transmit antennas, and the selection of orthogonal waveforms. Recently, IM has been utilized to design the integrated sensing and communication (ISAC) system by dynamically controlling the parameters of multi-dimensional waveforms according to the data flow, referred as IM-based ISAC [4–6, 16, 18, 24–27, 35, 36, 38–41]. The utilization of IM improves the waveform flexibility and provides a new perspective to the design of ISAC system. For communications subsystem, the data rate is increased by embedding additional information into the combinations of waveform parameters. For radar subsystem, frequency agile narrowband waveforms and sparse array can be employed to reduce the hardware complexity while leading to minimal reduction to the radar resolution [18, 24, 25, 27].

In recent years, many IM-based ISAC systems were proposed leveraging different waveform transmission strategies or antenna architecture. For waveform transmission, some schemes utilize the IM to facilitate the coexistence of separated coordinated signals [23, 25], while the other approaches aim to realize the dual functionalities by radiating joint waveforms [18, 27]. From the aspect of the antenna architecture, multiple kinds of array forms, including the phased array [18], multiple-input multiple-output (MIMO) array [16, 39] and the sparse array [27, 35], are utilized in the existing schemes. The proliferation of different IM-based ISAC systems makes it difficult to identify what scheme is most suitable for which scenario. In order to promote the development of the IM-based ISAC technique, it is necessary to sort out and summarize the current methods based on IM, so as to provide a guidance for future research.

The goal of this chapter is to review the IM-based ISAC systems. We begin by formulating a generic model and describing the general information embedding strategy, and discuss some existing IM-based ISAC schemes utilizing the generic model, identifying the differences of these schemes in the transmission model and information embedding strategy. We next introduce the signal processing algorithms for radar subsystems and communications subsystem. Subsequently, we introduce the performance metrics, and provides some simulation results based on these metrics. Finally, we conclude this chapter and discuss some possible research directions for IM-based ISAC systems.

2 Generic Model of IM-Based ISAC Systems

The ISAC system consists of an ISAC transmitter, a radar receiver and several communications receivers. An illustration of the ISAC system is depicted in Fig. 1. Typically, the ISAC transmitter and the radar receiver are located on the same device, whereas the communication receiver is remotely located [25]. The ISAC transmitter, the radar receiver, and the communications receiver are equipped with P, Q_{r}, and Q_{c} antenna elements, respectively.

To obtain the generic model of IM-based ISAC systems, we begin by introducing the transmission model in Sect. 2.1. Subsequently, we formulate the information embedding model based on the transmission model, and further discuss some specific IM-based ISAC systems in Sect. 2.2. Finally, the receive model of both radar and communications subsystems are derived in Sect. 2.3.

2.1 Transmission Model

A schematic transmission model is shown in Fig. 2. Let d_{T} denote the adjacent element distance of the transmit array. During each transmission cycle, the waveform $\check{x}_p(t)$ is multiplied with the weight a_p, and then transmitted from the pth element of the array. The weight a_p is a complex value, and may be varied between adjacent transmission cycles. When no waveform is transmitted from the pth antenna element, the transmit waveform is set as $\check{x}_p(t) = 0$. We next discuss how to construct

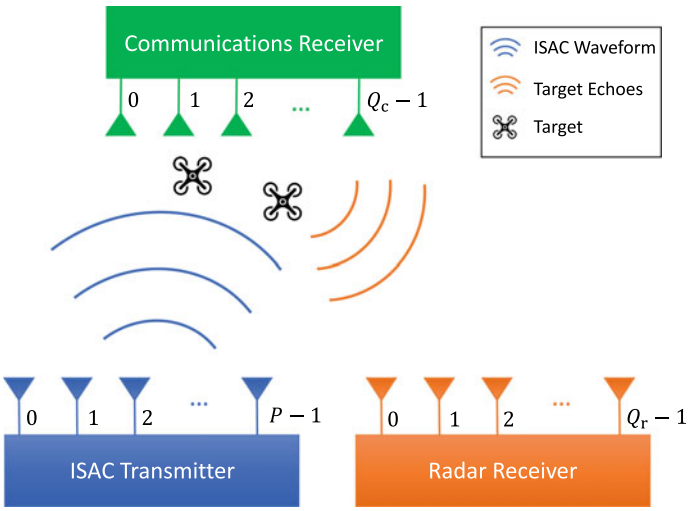

Fig. 1 An illustration of the ISAC system

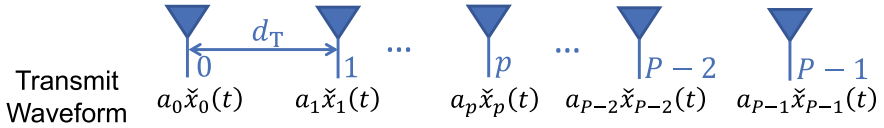

Fig. 2 An illustration of the ISAC transmission model

the transmit waveform, and illustrate how to embed the communication information into the transmit waveform.

Define the waveform set $\mathcal{X} = \{x_0(t), x_1(t), \ldots, x_{M-1}(t)\}$, where $\{x_m(t)\}$ are orthogonal to each other, and $m \in \{0, 1, \ldots, M-1\}$. The M waveforms in the set $\mathcal{X}$ can be combined into a waveform vector $\mathbf{x}(t)$, expressed as

$$\mathbf{x}(t) = \left[x_0(t), x_1(t), \ldots, x_{M-1}(t)\right]^T. \tag{1}$$

During each transmission cycle, K waveforms are first selected from the waveform set $\mathcal{X}$. Let $\tilde{x}_k(t)$ denote the kth selected waveform. The K selected waveforms can be composed into a set denoted by $\mathcal{X}_K = \{\tilde{x}_0(t), \tilde{x}_1(t), \ldots, \tilde{x}_{K-1}(t)\}$. Next, the K selected waveforms are combined in a vector, denoted by $\tilde{\mathbf{x}}(t)$, and expressed as

$$\tilde{\mathbf{x}}(t) = \left[\tilde{x}_0(t), \tilde{x}_1(t), \ldots, \tilde{x}_{K-1}(t)\right]^T. \tag{2}$$

The selection of the K waveforms can be described through the linear equation, given by

$$\tilde{\mathbf{x}}(t) = \Omega\mathbf{x}(t), \tag{3}$$

where Ω is a selection matrix of size $K \times M$. In each row of the matrix Ω, only one element equals the value 1, and the rest of elements equal 0. Then, the selected K waveforms are allocated to P transmit antennas according to a certain arrangement pattern. Let $\check{x}_p(t)$ denote the waveform assigned to the pth element of the antenna array. The waveforms assigned to the antennas are written as a vector given by

$$\check{\mathbf{x}}(t) = \left[\check{x}_0(t), \check{x}_1(t), \ldots, \check{x}_{P-1}(t)\right]. \tag{4}$$

Assume that the waveform $\tilde{x}_k(t)$ in $\mathcal{X}_K$ is assigned to be transmitted from L_k elements in the antenna array, where L_k is an integer no less than 1 and no larger than P. The process of assigning the selected K waveforms to the P transmit antennas can be described as the following equation

$$\check{\mathbf{x}}(t) = \Lambda\tilde{\mathbf{x}}(t), \tag{5}$$

where Λ is a distribution matrix of size $P \times K$. In each row of the matrix Λ, either all the entries equal 0, or only one entry equals 1 while the rest entries are 0. In the kth column of the matrix Λ, L_k entries are set to 1.

In order to convey the information through conventional symbols or realize the beamforming, the waveform assigned to each antenna is multiplied with the weight a_p, respectively. The generation of the weight a_p is as following: When the communication symbol is to be modulated on the waveform $\check{x}_p(t)$, a_p is the communication symbol; when the waveform $\check{x}_p(t)$ is beamformed to a desired direction, a_p is the weight required for beamforming; when there is no waveform transmitted from the pth transmit antenna, i.e., $\check{x}_p(t) = 0$, a_p is set to be 1. The weighting process can be expressed as $s_p(t) = a_p \cdot \check{x}_p(t)$, where $s_p(t)$ is the waveform transmitted from the pth antenna. This weighting process can also be written as a matrix form, expressed as

$$\mathbf{s}(t) = \mathbf{A}\check{\mathbf{x}}(t), \tag{6}$$

where $\mathbf{A}$ is a diagonal matrix of size $P \times P$, and can be expressed as

$$\mathbf{A} = \mathrm{diag}\left(\left[a_0, a_1, \ldots, a_{P-1}\right]\right). \tag{7}$$

Using (3), (5) and (6), the generation of the transmit waveform vector can be represented as the following equation

$$\mathbf{s}(t) = \mathbf{A}\Lambda\Omega\mathbf{x}(t). \tag{8}$$

In (8), the matrices Λ and Ω determines the selection pattern of the waveform and how the waveform is distributed among the antenna array. The diagonal entries of the matrix $\mathbf{A}$ is composed of the weights multiplied to the waveforms. In the following, we describe how to embed the communication information through the realization of matrices Λ, Ω and $\mathbf{A}$.

2.2 *Information Embedding Strategy*

The reviewed ISAC systems in this chapter embed the information bits through IM [2, 7, 12, 29]. Different from traditional modulation approaches that only convey bits through constellation symbols, such as quadrature amplitude modulation (QAM) and phase shift keying (PSK), IM conveys additional information in the indices of the building blocks of communication systems, such as the selection of transmit antennas [34, 43], sub-carriers [3, 9], and spreading codes [20]. In IM-based ISAC systems, the IM is employed to facilitate the coexistence of radar and communications in the spatial domain [28], and utilized to design the dual functional waveform through spatial index modulation [35], frequency index modulation [38, 39], or joint spatial-frequency index modulation [18, 27].

In this subsection, we first describe the generic model of information embedding strategy which is based on the IM. Subsequently, some existing IM-based ISAC schemes are discussed using this information embedding model.

2.2.1 Information Embedding Model

According to (8), it can be found that the vector of transmit waveform $\mathbf{s}(t)$ is obtained by sequentially multiplying the vector $\mathbf{x}(t)$ with the matrices Ω, Λ and $\mathbf{A}$, respectively. The information can be embedded into different kinds of waveform realizations by varying the selection of waveforms, the arrangement of the waveforms on antennas, and the multiplied weights on the waveforms. During the transmission, the data flow is split into several blocks, which can be utilized to control the selection of the matrices Ω, Λ and $\mathbf{A}$. Here, the communications bits carried by the waveform selection and the waveform arrangement on the transmit antenna are referred to IM bits, while the information carried by the multiplied weights are named as constellation bits. In the sequel, we describe how many bits can be embedded through IM and constellation in each transmission cycle, which can be a whole pulse [18, 27] or a single chip in a pulse [39].

Index Bits

We now derive the number of bits can be embedded in to IM with given waveform parameters. According the waveform generation process described in Sect. 2.1, there are $\binom{M}{K}$ combinations for the realizations of the selection matrix Ω, where $\binom{M}{K} := \frac{M!}{K!(M-K)!}$. For the allocation matrix Λ, the possible number of combinations is

$$\prod_{k=0}^{K-1} \binom{P - \sum_{k'=0}^{k} L_{k'-1}}{L_k}, \tag{9}$$

where we define $L_{-1} = 0$. Therefore, the number of bits that can be embedded through IM depend on the total number of realizations of the matrices Ω and Λ, which is given by

$$N_{\mathrm{IM}} = \lfloor \log_2 \binom{M}{K} \rfloor + \lfloor \log_2 \prod_{k=0}^{K-1} \binom{P - \sum_{k'=0}^{k} L_{k'-1}}{L_k} \rfloor, \tag{10}$$

where $\lfloor \cdot \rfloor$ is the integer floor operation.

Constellation Bits

The constellation bits are conveyed by traditional constellation symbols, which is realized by multiplying the diagonal entries of $\mathbf{A}$ to the waveforms $\check{\mathbf{x}}(t)$. Assume that among the P weights, D weights are realized as communication symbols, while the other $P - D$ weights are utilized for beamforming. If the order of the constellation symbol is J, then the number of bits can be carried by constellation symbol is

$$N_{\mathrm{Const}} = D \log_2 J. \tag{11}$$

2.2.2 Specific IM-Based ISAC Schemes

Spatial Modulation Based Coexistence

The spatial modulation based communication-radar (SpaCoR) system proposed in [28] implements the ISAC transmitter illustrated in Fig. 2 while incorporating IM in the form of generalized spatial modulation (GSM) [34]. By employing GSM, SpaCoR achieves increased communication rate while acquiring the same angle resolution as using the full antenna array for radar. The transmit array of SpaCoR is a uniform linear array. The transmit waveforms of radar and communications are orthogonal, and the waveform set $\mathcal{X}$ is expressed as $\mathcal{X} = \left\{s^{(\mathrm{r})}(t), s^{(\mathrm{c})}(t)\right\}$, where $s^{(\mathrm{r})}(t)$ is the radar waveform, $s^{(\mathrm{c})}(t)$ is the communication waveform without modulating symbols.

In SpaCoR, both the communication waveform and the radar waveform are selected for transmission. Therefore the selection matrix $\Omega = \mathbf{I}_2$. During the transmission of each waveform, $P_{\mathrm{T}}^{\mathrm{r}}$ antenna elements are utilized to transmit radar waveforms, while $P - P_{\mathrm{T}}^{\mathrm{r}}$ antenna elements are employed to transmit communication waveforms. The antenna allocation pattern between radar waveforms and communications waveforms can be utilized to convey information. This is achieved by changing the value of the allocation matrix Λ. According to the generic model provided in Sect. 2, the number of elements allocated to radar is $L_0 = P_{\mathrm{T}}^{\mathrm{r}}$, while the number of antenna elements assigned for communication is $L_1 = P - P_{\mathrm{T}}^{\mathrm{r}}$. Using (9), the allocation matrix Λ has a total of $\binom{P}{P_{\mathrm{T}}^{\mathrm{r}}}$ realizations. Therefore, the number of bits embedded through spatial index modulation is

$$N_{\mathrm{SM}} = \lfloor \log_2 \binom{P}{P_{\mathrm{T}}^{\mathrm{r}}} \rfloor. \tag{12}$$

To direct the radar beam to a desired direction θ, the weight multiplied to the radar waveform is set according to the principle of phased array [33, Chap. 8.2], i.e., $a_p = e^{j2\pi d \sin\theta/\lambda}$ if the pth antenna element is chosen to transmit the radar waveform during this cycle, where λ is the wavelength of the carrier frequency. In addition to embedding the information into spatial index modulation, the data bits can also be conveyed by traditional constellation symbols in SpaCoR. Therefore, $P_{\mathrm{T}}^{\mathrm{r}}$ diagonal entries of $\mathbf{A}$ are radar beamforming weights, while the other $D = P - P_{\mathrm{T}}^{\mathrm{r}}$ diagonal entries are communication symbols. Assume that the cardinality of the communications symbol is J, the number of bits conveyed by constellation modulation per transmission cycle is $D \log_2 J$. The total number of bits conveyed in each transmission cycle is

$$N_{\mathrm{SpaCoR}} = D \log_2 J + \lfloor \log_2 \binom{P}{P_{\mathrm{T}}^{\mathrm{r}}} \rfloor. \tag{13}$$

Hybrid Spatial-Frequency IM

In addition to using a single-dimensional index to carry information, it is also possible to jointly use multiple-dimensional indexes to design the waveforms of ISAC

systems. The literature [18] proposed the multi-carrier agile joint radar communication (MAJoRCom) system, which embeds the information through the selection of multi-carrier frequencies and the arrangement of these frequencies on the transmit antennas. MAJoRCom only utilizes radar waveforms chosen from an orthogonal waveform set. As a result, the communication message is conveyed only via IM, which includes the selection of the orthogonal waveforms to be transmitted (spectral IM) as well as in their division among the antenna elements (spatial IM).

In MAJoRCom, the transmit waveform set $\mathcal{X}$ is composed of M waveforms orthogonal in frequency, which is the same as the frequency hopping schemes, i.e., $\mathcal{X} = \left\{x_0^{(\mathrm{r})}(t)\right\}_{m=0}^{M-1}$, where $x_m^{(\mathrm{r})}(t) = x_{\mathrm{base}}(t)\, e^{j2\pi f_m t}$ denotes a radar waveform whose carrier frequency is f_m, and $x_{\mathrm{base}}(t)$ denotes the radar waveform in baseband. During the transmission of each cycle, K waveforms are first chosen from $\mathcal{X}$, thus the size of the waveform selection matrix Ω is $K \times P$. Each waveform is allocated to some antennas for transmission, and the number of elements allocated to the kth selected waveform is denoted by L_k. Therefore, there are L_k entries equaling 1 in the kth column of the allocation matrix Λ. In MAJoRCom, since the multiplied weights are utilized to direct the radar beam to the desired direction, the diagonal entries of the weight matrix $\mathbf{A}$ is generated according to the beamforming weights as in the phased array radar [33, Chap. 8.2].

The number of bits conveyed by MAJoRCom is determined by the possible number of realizations of the matrices Ω and Λ. In particular, the number of possible selection patterns in Ω is $\binom{M}{K}$, and the number of possible allocation patterns is

$$\prod_{k=0}^{K-1} \binom{P - \sum_{k'=0}^{k} L_{k'-1}}{L_k}, \tag{14}$$

where we define $L_{-1} = 0$. Therefore, the number of bits that can be carried in each cycle is given by

$$N_{\mathrm{MAJoRCom}} = \lfloor \log_2 \binom{M}{K} \rfloor + \lfloor \log_2 \prod_{k=0}^{K-1} \binom{P - \sum_{k'=0}^{k} L_{k'-1}}{L_k} \rfloor. \tag{15}$$

Hybrid Spatial-Frequency IM Combining PM

For the scenarios with limited hardware complexity and cost, a FMCW based joint radar-communications system (FRaC) was proposed to embed the data bits through hybrid IM combining phase modulation (PM). The FRaC system operates at reduced cost and complexity by transmitting using a reduced number of radio frequency (RF) modules, combined with narrowband frequency modulated continuous waveform (FMCW) signalling. This is achieved via array sparsification in transmission, formulating a virtual MIMO array by combining the signals in one coherent processing interval (CPI), in which the narrowband waveforms are transmitted according to the mapping rule of IM. In FRaC, communication information is conveyed by spatial-

frequency IM and PM. The IM is realized by controlling the selection of the transmit waveforms, which have different carrier frequency, and arranging the allocation pattern of the selected waveforms to the transmit array. The PM is accomplished by modulating the communication symbols on the transmit waveforms. In the following, we describe the transmit model of FRaC using the generic model, and describe the information embedding strategy.

In FRaC, the waveform set $\mathcal{X}$ is defined as $\mathcal{X} = \left\{x_{f_m}^{(\mathrm{r})}(t)\right\}_{m=0}^{M-1}$, where $x_{f_m}^{(\mathrm{r})}(t)$ represents the FMCW whose carrier frequency is f_m. At each transmission cycle, K waveforms are first selected from the set $\mathcal{X}$. Therefore, the selection matrix Ω has $\binom{M}{K}$ implementations. Then each selected waveform is allocated to 1 antenna for transmission, thus a total of K antennas are utilized for transmission, while the remaining $P - K$ antennas are not used for transmission. According to the generic model, it can be seen that the number of antennas allocated to each waveform is $L_k = 1$. Following (9), the number of possible realizations for the allocation matrix Λ is given by

$$\prod_{k=0}^{K-1} \binom{P-k}{1} = \binom{P}{K} \cdot K!. \tag{16}$$

The multiplied weights of FRaC are generated as PM symbols or equal to 1. When the pth antenna is chosen to transmit waveform, the corresponding weight a_p is selected from the set of PM symbols with an order of J. Since each transmit waveform is modulated to an independent symbol, the number of symbols conveyed in each transmission cycle is $D = K$, which conveys $K \log_2 J$ PM bits. In summary, the number of bits can be conveyed in each transmission cycle of FRaC is

$$N_{\mathrm{FRaC}} = \lfloor \log_2 \binom{M}{K} \rfloor + \lfloor \log_2 \binom{P}{K} \rfloor + \lfloor \log_2 K! \rfloor + K \log_2 J. \tag{17}$$

2.3 Receive Model

We next derive the receive models for both communications and radar subsystems in this subsection. These models are utilized in Sect. 3 for developing the signal processing algorithms.

2.3.1 Communication Receive Model

The communication receive model formulates the relationship between the transmit waveform and the receive communications signals. Consider that the communications receiver is synchronized with the ISAC transmitter, which can be realized by periodically transmitting preambles from the ISAC transmitter. For mathematical brevity, the channel response between the ISAC transmitter and the communications

receiver is assumed to follow the memoryless channel obeying flat fading, thus the channel state information can be expressed by a matrix denoted by $\mathbf{H} \in \mathbb{C}^{Q_c \times P}$. The entry located at the pth row and the q_cth column of $\mathbf{H}$ is denoted by h_{p,q_c}, which describes the channel response between the pth transmit antenna and the q_cth communications receive antenna. For the other kinds of channel responses, such as the frequency selection channel, the received signal model should be adjusted according the corresponding channel models [27].

Let $y_{q_c}^{(c)}(t)$ denote the signal received at the q_cth antenna of the communications receiver. The received signal $y_{q_c}^{(c)}(t)$ is given by

$$y_{q_c}^{(c)}(t) = \sum_{p=0}^{P-1} h_{q_c,p} \cdot a_p \cdot x_{m_p}(t) + w_{q_c}^{(c)}(t), \tag{18}$$

where m_p represents which waveform is transmitted in the pth transmit antenna. The continuous received signal is converted to the discrete format after sampling. Let T_s^c denote the sampling interval. The samples received at the q_cth antenna in the nth pulse are stacked as the vector

$$\mathbf{y}_{q_c}^{(c)} := \left[y_{q_c}^{(c)}[0], y_{q_c}^{(c)}[1], \ldots, y_{q_c}^{(c)}[U-1] \right]^{\mathrm{T}}, \tag{19}$$

where U denotes the number of received samples. The uth entry of $\mathbf{y}_{q_c}^{(c)}$ is given by

$$y_{q_c}^{(c)}[u] = \sum_{p=0}^{P-1} h_{q_c,p} \cdot a_p \cdot x_{m_p}[u] + w_{q_c}^{(c)}[u], \tag{20}$$

where $u \in \{0, 1, \ldots, U-1\}$, $w_n^{(c)}[u]$ is the white Gaussian noise with variance σ_c^2, and $x_p[u] := x_p\left(uT_s^c\right)$.

Using (20), $\mathbf{y}_{q_c}^{(c)}$ is rewritten as

$$\mathbf{y}_{q_c}^{(c)} = \Psi_{q_c}\mathbf{e} + \mathbf{w}_{q_c}^{(c)}, \tag{21}$$

where $\mathbf{e} \in \mathcal{E} \subset (\{\mathrm{diag}(\mathbf{A})\} \cup \{0\})^{PM}$ denotes the transmit symbol vector of the nth pulse in the ISAC transmitter. The selections of the waveforms. the arrangement pattern of the waveforms on the arrays, and the constellation symbols can be obtained from $\mathbf{e}$. The structure of $\mathbf{e}$ is given by

$$\mathbf{e} = \left[(\mathbf{e}_1)^{\mathrm{T}}, (\mathbf{e}_2)^{\mathrm{T}}, \ldots, (\mathbf{e}_M)^{\mathrm{T}} \right]^{\mathrm{T}}, \tag{22}$$

where $\mathbf{e}_m$ is a vector with size $P \times 1$. The entries of $\mathbf{e}_m$ is either all zero, or only has one non-zero entry at the pth entry if the waveform $s_{m_p}(t)$ is transmitted from the pth antenna. The value of this nonzero entry is $[e_m]_p = a_p$. The vector $\mathbf{w}_{q_c}^{(c)} := \left[w_{q_c}^{(c)}[0], \ldots, w_{q_c}^{(c)}[U-1] \right]^{\mathrm{T}}$ represents the additive noise. The matrix

$\Psi_{q_c} \in \mathcal{C}^{U \times PM}$ is comprised of $M-1$ sub-matrices, the size of which is $U \times P$, via

$$\Psi_{q_c} := \left[\boldsymbol{\psi}_{q_c,0}, \boldsymbol{\psi}_{q_c,1}, \cdots, \boldsymbol{\psi}_{q_c,M-1}\right]. \tag{23}$$

Each sub-matrix $\boldsymbol{\psi}_{q_c,m}$ is given by

$$\boldsymbol{\psi}_{q_c,m} := \left[\boldsymbol{\psi}^0_{q_c,m}, \boldsymbol{\psi}^1_{q_c,m}, \cdots, \boldsymbol{\psi}^{P-1}_{q_c,m}\right], \tag{24}$$

where $\boldsymbol{\psi}^p_{q_c,m} := h_{q_c,m}\mathbf{x}_m$, and $\mathbf{x}_m$ is the discrete sampling of the signal $x_m(t)$.

The signal received in all the antennas is stacked as the vector

$$\mathbf{y}^{(c)} := \left[\left(\mathbf{y}^{(c)}_0\right)^T, \left(\mathbf{y}^{(c)}_1\right)^T, \ldots, \left(\mathbf{y}^{(c)}_{Q_c-1}\right)^T\right]^T \tag{25}$$

By defining $\Psi := \left[\Psi_0^T, \Psi_1^T, \ldots, \Psi_{Q_c-1}^T\right]^T$, and

$$\mathbf{w}^{(c)} := \left[\left(\mathbf{w}^{(c)}_0\right)^T, \left(\mathbf{w}^{(c)}_1\right)^T, \ldots, \left(\mathbf{w}^{(c)}_{Q_c-1}\right)^T, \right. \tag{26}$$

the received signal is given by

$$\mathbf{y}^{(c)} = \Psi\mathbf{e} + \mathbf{w}^{(c)}. \tag{27}$$

The received signal model in (21) is utilized to formulate the decoding algorithm for recovering $\mathbf{e}$ from $\mathbf{y}^{(c)}$.

2.3.2 Radar Receive Model

The radar receive model describes the relationship between the radar received signal and the target parameters. To derive the radar receive model, L targets are assumed in the scenario. Let r_l, v_l, θ_l and β_l denote the range, the velocity, the angle, and the reflective factor of the lth target, respectively. One radar CPI is composed of N pulses. After down conversion by mixing with the carrier, the echoes received in each radar receive antenna are sampled into discrete signals. The echoes of the N transmit signals received in the Q_r antennas are combined into one signal denoted by $\mathbf{y}^{(r)}$, expressed as

$$\mathbf{y}^{(r)} = \sum_{l=0}^{L-1} \beta_l \tilde{\boldsymbol{\phi}}\left(\tilde{\mathbf{S}}(t), \boldsymbol{\theta}_l\right) + \mathbf{w}^{(r)}, \tag{28}$$

where $\tilde{\mathbf{S}}(t) := \left[\mathbf{s}_0(t), \mathbf{s}_1(t), \ldots, \mathbf{s}_{N-1}(t)\right]$ is composed by the signals transmitted in the N transmission cycles, $\mathbf{s}_n(t)$ is the signal vector transmitted in the nth transmission cycle, $\boldsymbol{\theta}_l := [v_l, r_l, \theta_l]$, $\mathbf{w}^{(r)}$ is the additive noise in the radar receiver, and

$\tilde{\boldsymbol{\phi}}\left(\tilde{\mathbf{S}}(t), \boldsymbol{\theta}_l\right)$ denotes the noiseless echo generated according to the parameters of the lth target. The expression of $\tilde{\boldsymbol{\phi}}\left(\tilde{\mathbf{S}}(t), \boldsymbol{\theta}_l\right)$ is generated according to the target parameter $\boldsymbol{\theta}_l$ and the shape of the antenna array, which is determined by the specific realization of ISAC systems. The readers can refer to [18, 25, 27] for detailed expressions.

To recover the parameters of radar targets, the range, velocity and angle are divided into $\tilde{M}$, $\tilde{N}$ and $\tilde{Q}$ grids, respectively, in the interest observation area. Typically, the interval between adjacent grids in each dimension is set according to the resolution in the corresponding dimension. The $\tilde{m}$th, $\tilde{n}$th and $\tilde{q}$th grid of the range, velocity and angle are denoted by $\tilde{r}_{\tilde{m}}$, $\tilde{v}_{\tilde{n}}$ and $\tilde{\theta}_{\tilde{q}}$, respectively, where $\tilde{m} \in \left\{0, 1, \ldots, \tilde{M}-1\right\}$, $\tilde{n} \in \left\{0, 1, \ldots, \tilde{N}-1\right\}$ and $\tilde{q} \in \left\{0, 1, \ldots, \tilde{Q}-1\right\}$. Assume that the targets are located on these grids. The target scene can be indicated by $\mathbf{B} \in \mathcal{C}^{\tilde{N}\times\tilde{M}\times\tilde{Q}}$ with entries

$$[\mathbf{B}]_{\tilde{n},\tilde{m},\tilde{q}} := \begin{cases} \beta_l, & \text{if exists } (v_l, r_l, \theta_l) = \left(\tilde{v}_{\tilde{n}}, \tilde{r}_{\tilde{m}}, \tilde{\theta}_{\tilde{\theta}}\right), \\ 0, & \text{otherwise.} \end{cases} \tag{29}$$

Following (28) and (29), it holds that

$$\mathbf{y}^{(\mathrm{r})} = \Phi\mathbf{b} + \mathbf{w}^{(\mathrm{r})}, \tag{30}$$

where $\Phi := \left[\boldsymbol{\phi}_0, \boldsymbol{\phi}_1, \ldots, \boldsymbol{\phi}_{\tilde{N}\tilde{M}\tilde{Q}-1}\right]$ is the observation matrix, $\mathbf{b}$ is the vectorized form of $\mathbf{B}$, i.e., $\mathbf{b}_{\tilde{n}\tilde{M}\tilde{Q}+\tilde{m}\tilde{Q}+\tilde{q}} = [\mathbf{B}]_{\tilde{n},\tilde{m},\tilde{q}}$. The $\tilde{n}\tilde{M}\tilde{Q} + \tilde{m}\tilde{Q} + \tilde{q}$th column of Φ is defined as

$$\boldsymbol{\phi}_{\tilde{n}\tilde{M}\tilde{Q}+\tilde{m}\tilde{Q}+\tilde{q}} := \tilde{\boldsymbol{\phi}}\left(\tilde{\mathbf{S}}(t), \boldsymbol{\theta}_{\tilde{n},\tilde{m},\tilde{q}}\right), \tag{31}$$

where $\boldsymbol{\theta}_{\tilde{n},\tilde{m},\tilde{q}} := \left[\tilde{v}_{\tilde{n}}, \tilde{r}_{\tilde{m}}, \tilde{\theta}_{\tilde{q}}\right]$.

3 Signal Processing

Joint radar and communications systems are required to realize the radar and communications functionalities by signal processing. For radar, it is necessary to recover the parameters of radar targets using the echoes. For communications, the received signal are processed to decode the message from the transmitter. In this section, the signal processing algorithms of radar and communications subsystems are introduced, respectively.

3.1 Communication Processing

We next discuss how the digital message is recovered from the communications receiver of the ISAC systems. In IM-based ISAC system, the information is decoded by recovering the index of the transmit waveforms as well as the symbols modulated on the waveform. In the sequel, we begin by formulating the received model of the communications receiver. Then we describe the maximum likelihood (ML) rule, which has the optimal performance for recovering the transmit message. Since ML algorithm may be computationally prohibitive, we also introduce an algorithm with reduced complexity building upon the inherent orthogonality of the waveforms.

3.1.1 Maximum Likelihood Algorithm

Assume that the receiver has full channel state information (CSI), i.e., knowledge of the matrix Ψ and the distribution of $\mathbf{w}^{(c)}$. The message can be decoded with minimal probability of error using the maximum a-posteriori probability rule. If the data bits are equiprobable, this symbol detection rule is given by

$$\hat{\mathbf{e}} = \arg\max_{\mathbf{e}\in\mathcal{E}} p\left(\mathbf{y}^{(c)}|\mathbf{e}, \Psi\right). \tag{32}$$

As the noise obeys a proper-complex white Gaussian distribution, it holds that (32) specializes to the minimum distance detector.

$$\hat{\mathbf{e}} = \arg\min_{\mathbf{e}\in\mathcal{E}} \|\mathbf{y}^{(c)} - \Psi\mathbf{e}\|_2^2. \tag{33}$$

In (32) and (33), the vector $\mathbf{e}$ is constructed according to the specific information embedding strategy realized in the ISAC system. Thus, recovering $\mathbf{e}$ via (32) generally involves searching over the set $\mathcal{E}$ whose cardinality is $2^{N_{\text{Total}}}$, where N_{Total} is the number of bits conveyed in each transmission cycle. This implies that the computational complexity grows with the dimensionality of the system, i.e., the number of antenna elements, as well as with the cardinality of the search space. To facilitate decoding, we next introduce a sub-optimal decoding algorithm with reduced complexity.

3.1.2 Low Complexity Decoding Algorithm

The high computational complexity of the ML detector follows from the need to search over the entire set $\mathcal{E}$. To decrease the complexity of detection, we introduce an algorithm with reduced complexity, which utilizes the orthogonality of the waveforms. The detection algorithm has two steps: First, the selection of the transmit waveforms is estimated via matched filtering. Then, the arrangement pattern of the

waveforms on the array and the symbols modulated on the waveforms are detected as detailed in the next.

Define $\boldsymbol{\psi}_m^p := \left[\left(\boldsymbol{\psi}_{0,m}^p\right)^{\mathrm{T}}, \left(\boldsymbol{\psi}_{1,m}^p\right)^{\mathrm{T}}, \ldots, \left(\boldsymbol{\psi}_{Q_{\mathrm{c}}-1,m}^p\right)^{\mathrm{T}}\right]^{\mathrm{T}}$, which is the $\big((m-1)P + p\big)$th column of Ψ. The received signal $\mathbf{y}_n^{(\mathrm{c})}$ is first matched with MP normalized filters. Each filter is given by $\tilde{\boldsymbol{\psi}}_m^p := \frac{\boldsymbol{\psi}_m^p}{\|\boldsymbol{\psi}_m^p\|_2}$. Define $\boldsymbol{\psi}_m := \left[\boldsymbol{\psi}_{0,m}^{\mathrm{T}}, \boldsymbol{\psi}_{1,m}^{\mathrm{T}}, \cdots, \boldsymbol{\psi}_{Q_{\mathrm{c}}-1,m}^{\mathrm{T}}\right]^{\mathrm{T}}$. The output of each matched filter is denoted by $g_m^p := \left(\tilde{\boldsymbol{\psi}}_m^p\right)^{\mathrm{H}} \mathbf{y}_n^{(\mathrm{c})}$. As the transmit waveforms are orthogonal to each other when $m \neq m'$, i.e., $\left(\tilde{\boldsymbol{\psi}}_m^p\right)^{\mathrm{H}} \boldsymbol{\psi}_{m'} = \mathbf{0}$, the output is expressed as

$$g_m^p = \left(\tilde{\boldsymbol{\psi}}_m^p\right)^{\mathrm{H}} \boldsymbol{\psi}_m \boldsymbol{e}_m + \left(\tilde{\boldsymbol{\psi}}_m^p\right)^{\mathrm{H}} \mathbf{w}^{(c)}. \tag{34}$$

Let $g_m^{\max}$ be the maximum amplitude output, i.e., $\left|g_m^{\max}\right| := \max_p \left|g_m^p\right|$. To identify the selected waveforms, the matched outputs $g_m^{\max}$ are sorted by descending order according to their amplitudes. Let $\{g_{m_0'}^{\max}, g_{m_1'}^{\max}, \cdots, g_{m_{K-1}'}^{\max}\}$ denote the K largest outputs that belong to the transmit waveform set, then the estimated index of the transmit waveforms, denoted by $\{\hat{m}_k\}$, are obtained via $\hat{m}_k = m_k'$.

After determining the selected transmit waveforms, the receiver needs to further estimate the arrangement pattern of the waveform on the array, and the constellation symbols modulated on each waveform. Once the selected transmit waveforms have been found, detection of the waveform arrangement pattern and the constellation symbols are carried out by searching over the subset $\mathcal{E}_{\mathrm{sub}} \subset \mathcal{E}$, which is composed of all vectors $\mathbf{e}$ corresponding to the transmission patterns that transmit waveforms with the detected carrier frequencies. The estimation is expressed as

$$\hat{\mathbf{e}} = \arg\min_{\mathbf{e} \in \mathcal{E}_{\mathrm{sub}}} \|\mathbf{y}^{(\mathrm{c})} - \Psi \mathbf{e}\|_2^2. \tag{35}$$

Neglecting the computation in the first step, the computational complexity is reduced by a factor of $2^{\lfloor \log_2 \binom{M}{K} \rfloor}$ compared to the ML rule, as the cardinality of $\mathcal{E}$ is $2^{\lfloor \log_2 \binom{M}{K} \rfloor}$ times the cardinality of $\mathcal{E}_{\mathrm{sub}}$.

3.2 Radar Processing

The task of radar detection is to recover the range, velocity and angle of the targets. In the next, we first derive the receive model of the radar subsystem. Then we introduce the radar detection algorithms according to different conditions of the receive model.

3.2.1 Radar Detection Algorithm

The range, velocity and angle can be estimated by recovering $\mathbf{b}$ from the observation function (30). According to the specific implementation approach of the integrated system, the observation equation in (30) can be classified into two types. The first type transmits broadband waveforms through a full array. Therefore, the radar range resolution and angle resolution are realized without bandwidth synthesizing or aperture synthesizing. In this condition, the observation equation is well-determined or over-determined, i.e., the number of rows in the observation matrix Φ is no less than the number of columns, and the rank of Φ equals $\tilde{N}\tilde{M}\tilde{Q}_{\mathrm{r}}$. In the second type of observation equation, sparse arrays or frequency agile narrowband waveforms are utilized, thus the radar range resolution or the angle resolution are enhanced by synthesizing a wide bandwidth or a large aperture through signal processing. In this condition, the observation equation (30) is under-determined, i.e., the number of rows of the observation equation is less than the number of columns.

According to the above classifications to the observation equation, we next introduce the target recovery algorithms. We begin by introducing the matched filtering method which is suitable to solving both the well-determined/over-determined equations and the under-determined equations. In the next, we describe the target recovery algorithms which are only suitable to solve the well-determined/over-determined condition or the under-determined conditions, respectively.

Matched Filtering

Traditional radar utilizes matched filtering to detect the target echoes contaminated by noise [31, Chap. 4.2]. The matched filtering is realized by the correlation of the received echo and the reference signal, which is generated as the noiseless echo with respect to specific target parameters. Note that, in (30), the column of the observation matrix Φ is defined as the noiseless echo in terms of the parameters on the grid of $\mathbf{b}$. Hence, the matched filtering method can be calculated by multiplying Φ^{H} to the received signal, i.e.,

$$\hat{\mathbf{b}} = \Phi^{\mathrm{H}}\mathbf{y}^{(\mathrm{r})}. \tag{36}$$

The advantage of the matched filtering method is that the computational complexity is low, and it can be utilized to solve both the well-determined/over-determined and the under-determined cases. Nonetheless, when the matched filtering is utilized to solve the under-determined observation equations, a relative high side-lobe may be generated by the sparsity of the waveforms in frequency or array aperture, which may lead to obvious interference between multiple targets.

Well-Determined/Over-Determined Cases

When the observation equation is well-determined or over-determined, the recovery of $\mathbf{b}$, denoted by $\hat{\mathbf{b}}$, can be directly solved by the ML algorithm, i.e.,

$$\hat{\mathbf{b}} = \arg\max_{\mathbf{b}} p\left(\mathbf{y}^{(\mathrm{r})}|\mathbf{b}\right). \tag{37}$$

Under the additive white Gaussian noise assumption, the ML estimation can be obtained by minimizing the following cost function given by

$$\hat{\mathbf{b}} = \arg\min_{\mathbf{b}} \|\mathbf{y}^{(\mathrm{r})} - \Phi\mathbf{b}\|_2^2. \tag{38}$$

The minimizing of (38) is the least squares problem, the solution of which is given by [21, Chap. 8]

$$\hat{\mathbf{b}} = \left(\Phi^{\mathrm{H}}\Phi\right)^{-1}\Phi^{\mathrm{H}}\mathbf{y}^{(\mathrm{r})}. \tag{39}$$

Under-Determined Cases
When (30) is an under-determined problem, the recovery of $\hat{\mathbf{b}}$ can be solved using sparse recovery methods considering the sparsity of $\mathbf{b}$, which is often assumed in the radar studies [17, 19]. The sparse recovery problem is formulated as

$$\min_{\mathbf{b}} \|\mathbf{b}\|_0, \text{ subject to } \|\mathbf{y}^{(\mathrm{r})} - \Phi\mathbf{b}\| \leq \epsilon, \tag{40}$$

where ϵ is related to the noise level. The optimization problem (40) can be solved by compressed sensing (CS) algorithms, such as greedy approaches and ℓ_1 relaxation-based optimization [10, 13]. One can increase the speed of solving (40) by utilizing hardware accelerators, e.g., graphics processing units. Furthermore, recent advances in deep learning for CS have shown that model-based and structured neural networks can be trained to rapidly solve problems of the form of (40) [32], e.g., via deep unfolding of sparse recovery algorithms [15].

4 System Performance

We next evaluate the performance of IM-based ISAC systems, including the performances of the radar subsystem and communication subsystems. For each subsystem, we first introduce the metrics to measure the performance, and then utilize the introduced metrics to evaluate the performance of some existing IM-based ISAC systems.

4.1 Radar Performance

In the following, we first characterize the radar ambiguity function in Sect. 4.1.1, which can be utilized to evaluate the resolutions of the radar subsystem. Then, we study the relationship between the maximum number of recoverable targets and the waveform parameters using the theory of phase transition in Sect. 4.1.2.

4.1.1 Ambiguity Function

The ambiguity function is a useful measure for characterizing the radar resolution and the mutual interference between multiple targets [31, Chap. 4]. The ambiguity function is defined as the correlation of the noiseless received signal and the reference signal. In particular, the parameters of the receive signal are $\{\beta = 1, \boldsymbol{\theta} = [r, v, \theta]\}$, and the parameters of the reference signal are $\{\beta = 1, \boldsymbol{\theta} = [r_{\text{ref}}, v_{\text{ref}}, \theta_{\text{ref}}]\}$. Using the definition in Sect. 2.3.2, the received signal and the reference signal are denoted by $\tilde{\phi}\left(\tilde{\mathbf{S}}(t), \theta\right)$ and $\tilde{\phi}\left(\tilde{\mathbf{S}}(t), \boldsymbol{\theta}_{\text{ref}}\right)$, respectively. Thus, the expression of the ambiguity function, denoted by $\chi(\delta r, \delta v, \delta\theta)$, is written as

$$\chi(\delta r, \delta v, \delta\theta) = \tilde{\phi}^H\left(\tilde{\mathbf{S}}(t), \boldsymbol{\theta}_{\text{ref}}\right)\tilde{\phi}\left(\tilde{\mathbf{S}}(t), \boldsymbol{\theta}\right), \tag{41}$$

where $\delta r := r - r_{\text{ref}}$, $\delta v := v - v_{\text{ref}}$, and $\delta\theta := \theta - \theta_{\text{ref}}$.

Since the transmit waveform and the antenna allocation pattern are determined by the transmitted message, the ambiguity function is a random quantity which takes a different realization on each CPI. To study the performance of the radar subsystem, the stochastic properties of the ambiguity function are often evaluated, as done in [17, 25, 27]. The analysis in [25, 27] indicates that when the transmit waveform is randomly chosen in the frequency domain or in the antenna domain, the expectation of the ambiguity function is identical to that of the systems transmitting wideband waveform or using full antenna array. Thus the randomization in the spatial enables to reduce the hardware complexity by using less radio frequency modules, while the randomization in frequency domain decreases the instantaneous bandwith, without affecting the radar resolution. For a CPI with a finite number of pulses, the difference between the random instantaneous ambiguity function and its expected value is dictated by its variance [30, Chap. 5]. The variance of the ambiguity function is studied in [25], which shows that the variance decreases when the number of pulses increases. Since the variance can indicate the side-lobe level of the ambiguity function. The analysis in [25] also indicates that the side-lobe level decreases with the increasing of the number of pulses in one CPI.

We next show how to utilize the ambiguity function to evaluate the performance of radar subsystem. In particular, we take the FRaC system [27] as an example. We empirically evaluate the ambiguity function of FRaC, and compare it with the theoretical expected ambiguity function provided in [27]. To show the ambiguity function of FRaC, a single realization of the ambiguity function is calculated. Since the ambiguity function has three arguments, two cross sections of the ambiguity function at $\chi(\delta f_r, 0, \delta f_\theta)$ and $\chi(0, \delta f_v, \delta f_\theta)$ are shown in Figs. 3a, b, respectively. For comparison, we depict the theoretical expected ambiguity function in Fig. 3c, d. Here, f_r, f_v and f_θ denote the normalized range, velocity and angle frequencies, which is linear related to the values of range, velocity and angle, respectively, and the expression. To obtain the detailed expressions of the normalized frequencies, please refer to [27].

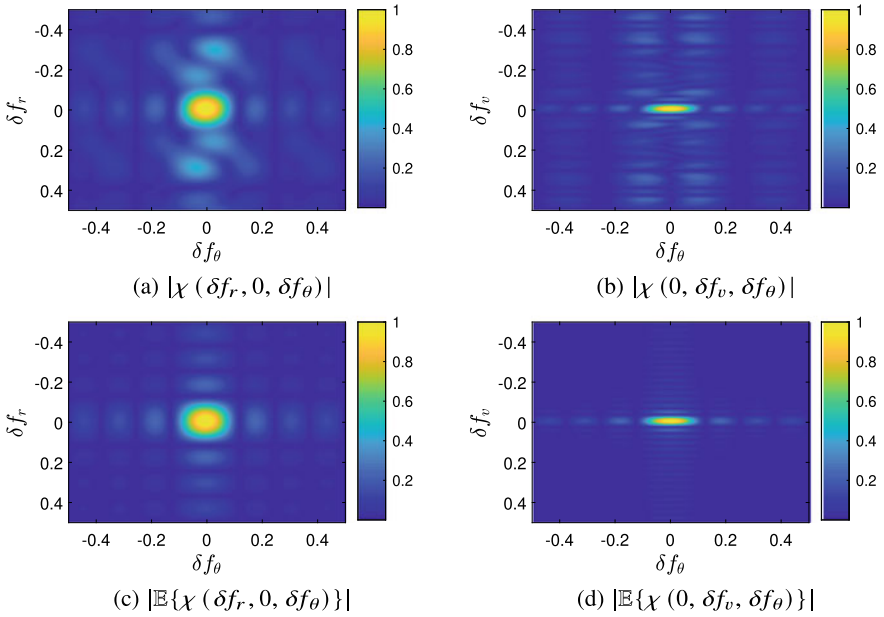

(a) $|\chi(\delta f_r, 0, \delta f_\theta)|$ (b) $|\chi(0, \delta f_v, \delta f_\theta)|$

(c) $|\mathbb{E}\{\chi(\delta f_r, 0, \delta f_\theta)\}|$ (d) $|\mathbb{E}\{\chi(0, \delta f_v, \delta f_\theta)\}|$

Fig. 3 Numerically evaluated ambiguity functions. Readers can refer to detailed simulation parameters from Fig. 5 of [27]

The similarity between the instantaneous ambiguity function and its theoretically evaluated expectation is observed in Fig. 3. The resolution is obtained from the width of the mainlobe. Comparing Fig. 3a–d, we find that the mainlobe width of both ambiguity functions are nearly the same. According to the analysis in [27], the mailobe width of the expected ambiguity function of FRaC equals to that of the system which transmit a wideband waveform and using a large antenna array [37, Chap. 2.10]. This indicates that the randomization in the antenna selection and the frequency division, which FRaC utilizes to embed communication messages and reduce hardware complexity, also contributes to its resolution.

4.1.2 Phase Transition Threshold

Ambiguity function can be utilized to analyze the resolution and the sidelobe level of the radar subsystem. Nonetheless, ambiguity function cannot provide an accurate recovery performance with respect to the transmit waveform. When the observation function is well-determined/over-determined, the radar recovery accuracy can be analyzed through the classical statistical theory, such as the Cramér lower bound [21]. However, the theory to analyze the recovery accuracy of the under-determined observation equations is still an emerging research. For this purpose, we introduce the phase transition theory [1], which is a breakthrough in evaluating the recovery accuracy of

the under-determined observation equations, in this section. In CS, phase transition thresholds divide the plane of parameters into regions where recovery succeeds and fails with high probability. Although existing phase transition results are focused on Gaussian matrices, numerical simulations have been utilized to show that such an analysis also reflects on radar systems whose recovery can be expressed as CS with structured measurement matrices, such as frequency agile radar (FAR) [22]. In the sequel, we introduce the application of the phase transition theory to analyze the radar subsystem of the IM-based ISAC system. By doing so, the number of recoverable targets is characterized as a function of the waveform parameters.

We begin by providing some preliminaries on phase transition in the context of CS. Consider an under-determined problem $\mathbf{y} = \Omega\mathbf{x}$, where $\mathbf{y} \in \mathcal{C}^{N_1}$, $\Omega \in \mathcal{C}^{N_1 \times N_2}$ is a complex Gaussian matrix, and $\mathbf{x} \in \mathcal{C}^{N_2}$ is a sparse vector with N_s nonzero entries. CS recovers $\mathbf{x}$ by solving the following optimization problem

$$\min_{\mathbf{x}} \|\mathbf{x}\|_0, \text{ subject to } \mathbf{y} = \Omega\mathbf{x}, \tag{42}$$

which is typically relaxed into an ℓ_1 norm minimization [13],

$$\min_{\mathbf{x}} \|\mathbf{x}\|_1, \text{ subject to } \mathbf{y} = \Omega\mathbf{x}. \tag{43}$$

Problem (43) is convex, and its recovery limits can be characterized using the phase transition theory. The phase transition threshold of (43) indicates the maximum sparse degree, denoted by N_s^*, for a given N_1 and N_2. This threshold is the demarcation point that separates the successful recovery and failing recovery with high probability. Namely, when $N_s \leq N_s^*$, $\mathbf{x}$ can be recovered with high probability, while when $N_s > N_s^*$, the probability of exact recovery dramatically decreases. The phase transition threshold of solving (43) can be computed via the following lemma [22]:

Lemma 1 *The sparse vector* $\mathbf{x}$ *can be exactly recovered via* (43) *with high probability, when* $N_s \leq N_s^*$, *where* N_s^* *is related to* N_1 *and* N_2 *via*

$$N_1 = \inf_{\gamma \geq 0} \frac{1}{2}\left\{ N_s^* \left(2 + \gamma^2\right) + \left(N_2 - N_s^*\right) \int_{\beta}^{\infty} (u - \gamma)^2 \phi_2(u)\, \mathrm{d}u \right\}, \tag{44}$$

where $\phi_2(u) = ue^{-u^2/2}$.

Using Lemma 1, we can obtain the target recovery performance of IM-based ISAC systems, which may employ the frequency IM or spatial IM. In particular, we consider a noiseless scenario, as commonly assumed in such studies [1, 11, 14], i.e., the noise term in (30) is omitted. In this case, the target recovery problem formulated in (40), tackled via ℓ_1 norm minimization, is given by the convex problem

$$\min_{\mathbf{b}} \|\mathbf{b}\|_1, \text{ subject to } \mathbf{y}^{(\mathrm{r})} = \Phi\mathbf{b}. \tag{45}$$

The main difference between (43), used in Lemma 1, and (45), is in the structure of measurement matrices. Although phase transition results such as Lemma 1 assume Gaussian measurements, it was numerically shown that the analysis for Gaussian matrices is also accurate for structured measurements which arise in FAR [22].

The phase transition threshold of (45) indicates the maximum number of exactly recovered targets, denoted by L^*, for given waveform parameters. An application of the phase transition theory to analyze the target recovery with respect to the waveform parameters is provided in [27], which indicates the maximum number of recoverable targets for given waveform parameters, i.e., pulse number N, number of active antennas K, amount of available transmit antennas P, number of sub-carriers M, and amount of radar receive antennas Q_{r}. In particular, when the number of targets obeys $L \leq L^*$, then they can be exactly recovered with high probability, while when $L > L^*$, the probability of exact recovery dramatically decreases. The relationship between this threshold and the ISAC waveform $\{N, K, M, P, Q_{\mathrm{r}}\}$ is obtained from Lemma 1 as stated in the following corollary [27]:

Corollary 1 *For a given* $\{N, K, M, P, Q_{\mathrm{r}}\}$*, the phase transition threshold* L^* *for* (45) *with Gaussian measurements* $\mathbf{\Phi}$ *satisfies*

$$NKQ_{\mathrm{r}} = \inf_{\gamma \geq 0} \frac{1}{2} \Big\{ L^* \left(2 + \gamma^2\right) + \left(NMPQ_{\mathrm{r}} - L^*\right) \int_{\beta}^{\infty} (u - \gamma)^2 \phi_2(u) \, \mathrm{d}u \Big\}. \tag{46}$$

To show that the threshold is accurate to reveal the target recovery performance with respect to the waveform parameters, the simulated phase transition threshold is compared with the theoretical quantities computed via (46). The simulated phase transition threshold is observed from the behavior of recovery probability curve versus the number of targets, as shown in Fig. 4. We observe in Fig. 4 that, for each waveform parameter setting, the exact recovery probability drastically decreases around the theoretical threshold of (46). Thus, the phase transition can be obtained by theoretical calculation, while accurately reflecting the empirical performance. For other IM-based ISAC systems, the target recovery performance can also be obtained by substituting specific waveform parameters into (44).

4.2 Communication Performance

The communications performance of the ISAC systems can be evaluated by the bit error rate (BER) and the achievable rate. Since there is no close form expression of the BER and achievable rate for the proposed generic model of IM-based ISAC systems, we evaluate the performance of the IM-based ISAC system through simulation in this section. Through the simulation, we show that the communication performance is improved by embedding additional bits through IM. This gain follows from the fact

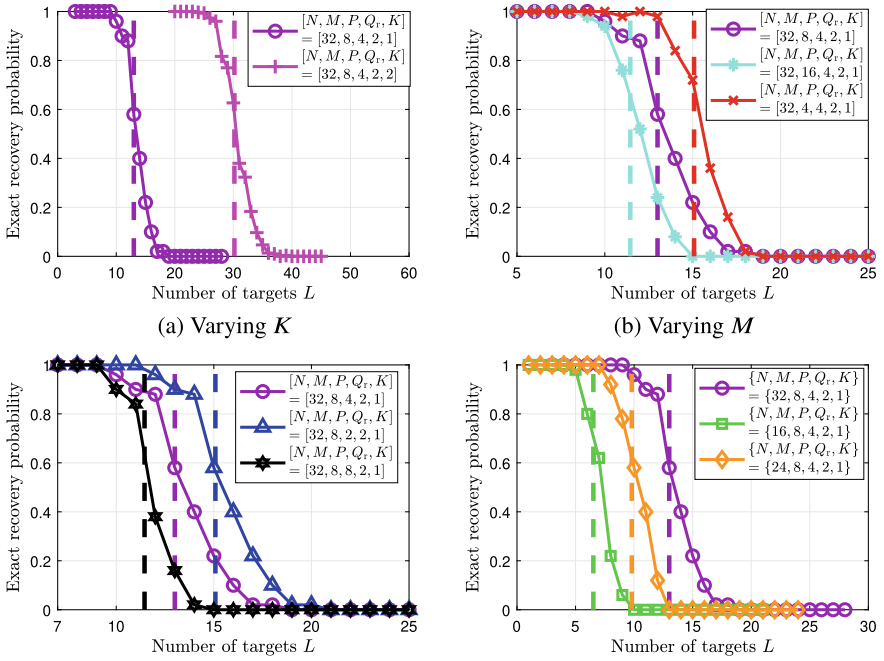

(a) Varying K (b) Varying M

(c) Varying P (d) Varying N

Fig. 4 Exact recovery probabilities versus the number of targets. In each subfigure, only one waveform parameter varies, i.e. varying K in (a), varying M in (b), varying P in (c) and varying N in (d). The vertical dash lines describe the locations of the theoretical phase transition thresholds of the corresponding waveform parameters indicated by different colors

that IM utilizes less denser constellations compared to the traditional scheme with the same data rate. To that aim, the FRaC system proposed in [27], the MAJoRCom system proposed in [18], and the ISAC system, which only exploits PM for data conveying, are compared. For these schemes, the achievable rate and the uncoded BER are utilized as the performance measures.

4.2.1 Achievable Rate

We numerically compare the achievable rates of FRaC, MAJoRCom and the wide-band FMCW with PM. Following [42], the achievable rate is computed via

$$I\left(\mathbf{e}; \mathbf{y}^{(\mathrm{c})}\right) = -Q_{\mathrm{c}} \log_2 e - \mathbb{E}_{\Psi}\left\{\mathbb{E}_{\mathbf{y}^{(c)}|\Psi}\left\{\log_2\left(\frac{1}{|\mathcal{E}|}\sum_{\mathbf{e}\in\mathcal{E}} e^{\frac{-\|\mathbf{y}^{(\mathrm{c})}-\Psi\mathbf{e}\|_2^2}{\sigma_{\mathrm{c}}^2}}\right)\right\}\right\}. \tag{47}$$

The stochastic expectations are computed via empirical averaging. Similarly, the achievable rates of MAJoRCom and the compared PM scheme are obtained by substituting the corresponding input vector into (47).

To compare the achievable rates of FRaC and the PM-only based scheme, we keep the data rates of FRaC and the compared PM system to be the same, using 6 bits/pulse and 7 bits/pulse. The waveform parameters are configured as $\{M, P, Q_c, K\} = \{8, 4, 4, 1\}$. As FRaC uses IM to convey $N_{\text{IM}} = \lfloor \log_2 \binom{M}{K} \rfloor + \lfloor \log_2 \binom{P}{K} \rfloor + \lfloor \log_2 K! \rfloor = 5$ bits per pulse, binary phase shift keying (BPSK) and quadrature phase shift keying (QPSK) are utilized to realize the data rates of 6 bits/pulse and 7 bits/pulse, respectively. The PM-only based benchmark thus utilizes the constellations of orders 64 and 128, to convey the same amounts of 6 bits/pulse and 7 bits/pulse, respectively. To compare the achievable rates of FRaC and MAJoRCom in a fair manner, the number of RF modules in the transmitter are set as the same in FRaC and MAJoRCom. To meet this condition, we also simulate FRaC with the waveform parameters of FRaC configured as $\{M, P, Q_c, K, J\} = \{8, 4, 4, 2, 2\}$, while the waveform parameters of MAJoRCom are set as $\{M, P, Q_c, K, L_K\} = \{8, 2, 4, 2, 1\}$. With this parameter setting, according to (17) and (15), the data rates of FRaC and MAJoRCom are $\lfloor \log_2 \binom{M}{K} \rfloor + \lfloor \log_2 \binom{P}{K} \rfloor + \lfloor \log_2 K! \rfloor + \log_2 J = 9$ bits/pulse and $\lfloor \log_2 \binom{P}{K} \rfloor + \lfloor \log_2 \frac{P!}{(P_K!)^K} \rfloor = 5$ bits/pulse, respectively.

The evaluated achievable rates are depicted in Fig. 5. Observing Fig. 5, we note that, as expected, the achievable rate does not exceed the cardinality of $\mathcal{E}$, i.e., the maximal rates of FRaC-K1-BPSK and 64-BPSK are 6 bits/pulse, while the maximal rates of FRaC-K1-QPSK and 128-BPSK are 7 bits/pulse. However, these rates are only achieved at high signal-to-noise ratio (SNR) values. In low SNRs, the achievable rates of FRaC outperform that of the PM wideband FMCW, indicating the improved spectral efficiency of combining IM with PM in ISAC signalling. We also observe in Fig. 5 that the rates achieved in FRaC-K2-BPSK are higher than that of the MAJoRCom in all considered SNRs. As expected, in high SNRs, the maximal achievable rates of FRaC-K2-BPSK and MAJoRCom approaches 9 bits/pulse and 5 bits/pulse, respectively. This is because more bits can be embedded in FRaC by utilizing the sparse array and combining the PM. These results indicate FRaC can convey more information than MAJoRCom while utilizing the same number of RF modules.

4.2.2 Bit Error Rate

We next evaluate the uncoded BER performance of the communications subsystem using the same setups in the achievable rate evaluations. In this experiment, a total of 10^5 ISAC waveforms are generated and decoded for each SNR value. The numerically evaluated BER results of FRaC, the PM scheme and MAJoRCom are shown in Fig. 6. As in the achievable rate study, we compare the BER curves of FRaC-K1-BPSK, FRaC-K1-QPSK, and FRaC-K2-BPSK with that of 64-PSK, 128-PSK, and MAJoRCom, respectively. Observing Fig. 6, we find that the BER performances of FRaC significantly outperform that of the PM system. These improvements stem

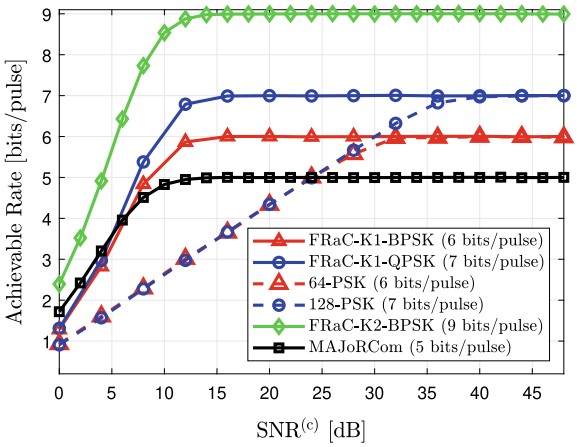

Fig. 5 Achievable rate comparison. Readers can refer to detailed simulation parameters from the simulation of Fig. 11 in [27]

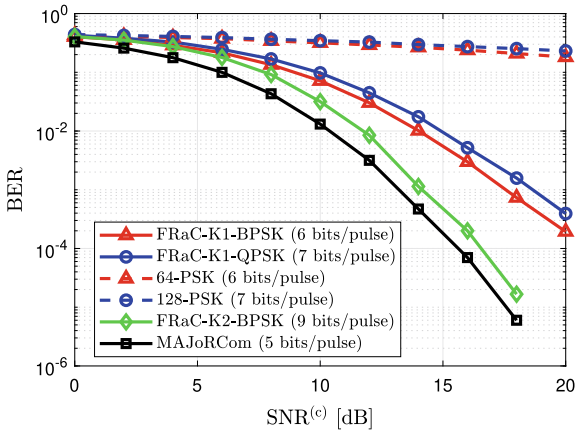

Fig. 6 BER comparison. Readers can refer to detailed simulation parameters from the simulation of Fig. 12 in [27]

from the fact that FRaC uses less dense PM constellations, since it conveys additional bits through IM. Comparing the BER curves of FRaC-K2-BPSK with MAJoRCom, we note that FRaC-K2-BPSK, which conveys almost twice the amount of bits as that of MAJoRCom for the considered setup, achieves BER within an SNR gap of merely 1 dB, indicating on its ability to achieve higher data rates using coded transmissions.

4.3 Performance Tradeoff Between Radar and Communications

To show the tradeoff between the performances of radar and communications subsystems, we jointly evaluate the aforementioned performance metrics of both subsystems by simulation. Here, the performance of the ISAC system proposed in [27]

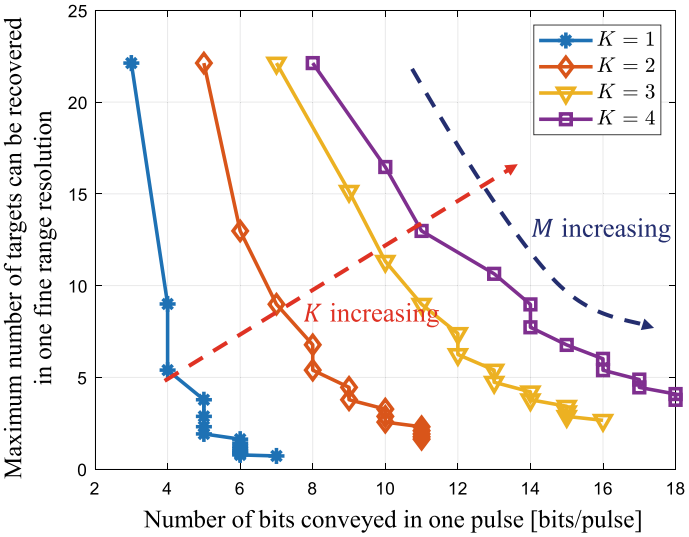

Fig. 7 The performance trade-off between radar and communications versus different waveform parameters. For each curve, M increases from $M = K$ to $M = 16$. The number of transmit antenna elements is set as $P = 4$, and BPSK is utilized to generate the modulated symbols. The number of pulses in one CPI, the number of transmit elements and radar receive elements are set as $N = 32$, $P = 4$, and $Q_{\mathrm{r}} = 2$, respectively. The other parameters are set the same as those in Fig. 4

is evaluated. The performance of radar is measured by the maximum number of recoverable targets and calculated according to equation (46). The communication performance is measured by the number of bits transmitted by each pulse, which can be calculated according to equation (17). In the simulation, for each curve, the number of subcarriers, denoted by M, increases from $M = K$ to $M = 16$, where K is the number of active subcarriers. The number of transmit antenna elements is set as $P = 4$, and BPSK is utilized to generate the modulated symbols.

The vertical axis of Fig. 7 shows the maximum number of targets that can be accurately recovered by each fine range resolution, and the horizontal axis shows the number of bits conveyed in each pulse. As can be seen from Fig. 7, when the other waveform parameters remain unchanged, dividing the frequency band into more subcarriers, i.e., increasing M, improves the communication rate, but will lead to a degradation to the number of recoverable targets. This is because increasing the total number of subcarriers leads to a sparser transmission in the frequency domain. When other parameters remain unchanged, increasing the number of active array elements K, which is also the number of active subcarriers, achieves better performances both in radar and communications. This is because with the waveform parameters in this simulation, the increase of K enables to embed more bits through IM and constellation modulation. The performance improvement in the maximum number of recoverable targets is because more measurements are observed in the frequency domain and antenna domain.

4.4 Discussion

The performance metrics discussed in this section can be utilized to evaluate the performance of the ISAC systems and guide the waveform design of practical systems. Among these metrics, ambiguity function can be utilized to evaluate the resolution and sidelobe level. The phase transition is a useful tool to design the waveform parameters according to the maximum number of targets in the scenario. As for the BER and achievable rate for communications subsystem, these performances are related to the realistic channel state. In addition, when the system needs to be deployed in a real environment, some practical problem should be considered, such as the errors existed in real synchronization and channel estimation.

Using these performance metrics, we evaluated the performance of some existing IM-based ISAC systems, such as FRaC and MAJoRCom. From these analysis and simulations, we find that utilizing IM improves the waveform flexibility, and achieves a good tradeoff among the radar performance, communications performance, and the hardware complexity. In particular, the dynamic variation in the carrier frequency and the active antenna elements enable to reduce the hardware complexity without degrading the radar resolution. For communications, the additional bits embedded into the combinations of waveform parameters enables to increase the data rate or improve the reliability.

5 Conclusions and Future Challenges

The utilization of IM improves the waveform flexibility, and achieves a good tradeoff among the radar performance, communications performance and the system complexity, making it an attractive approach for ISAC systems. In this chapter, we first formulated a generic model for IM-based ISAC systems. Based on the generic model, we discussed the signal models and information embedding strategies for some specific ISAC systems utilizing IM in different domains, including spatial modulation based coexistence, hybrid frequency-spatial IM, and hybrid spatial-frequency IM combining PM. Then we introduced the signal processing algorithms for radar and communications subsystems, respectively. For communications subsystem, we introduced the optimum ML detection algorithm, and the low complexity algorithm which adopts the orthogonal property of the waveforms. For radar subsystem, the observation equations are classified into the well-determined/over-determined cases and the under-determined cases. The radar signal processing algorithms of both cases were introduced. To analyze the performance of ISAC systems, the ambiguity function as well as the phase transition are utilized as the radar metrics, and the BER and achievable rate are employed to evaluate the communication performance. We evaluated the performances of some IM-based ISAC systems using these metrics, which shows that the utilization of IM enables to save the spectral and hardware resources

while leads to minimal influence to the radar resolution, and the communications performance is improved by embedding additional bits through IM.

While recent years have witnessed a rapid development on IM-based ISAC systems, there still give rise to a multitude of unexplored research directions. On the theoretical side, the performance metric, for the radar subsystems having underdetermined observation equations, is derived in noiseless scenario. Traditional radar performances measured in the noise condition, such as the detection probability and the estimation accuracy, remain to be studied. The lack of a closed form expression of the BER and achievable rate makes it difficult to evaluate the communications performance in an efficient manner. In addition, the current performance metrics on IM-based ISAC systems cannot directly reveal the tradeoff between radar and communication performance. A unified performance metric for multiple functionalities will uncover the fundamental limits of ISAC designs, characterizing their optimal gain over well-studied separate systems. From the perspective of algorithm, at present the signal processing of communication is mainly focused on decoding. It is necessary to study the synchronization and channel estimation algorithms to promote the practical deployment of the ISAC systems. As for the radar signal processing, since the target parameters are discretized into several grids, the continuous target parameters may mot exactly located in the grids, i.e., the off-grid phenomenon. Advanced algorithms, such as atomic norm minimization [8], can be investigated to solve the off-grid target recovery problem. Finally, on the practical side, the system constraints such as sampling rate and receiving bandwidth in the receiver should be considered in the future investigations. Additionally, the ISAC systems should be tested in real scenarios in order to facilitate the translation from theory to practical applications.

References

1. Amelunxen, D., Lotz, M., McCoy, M.B., Tropp, J.A.: Living on the edge: phase transitions in convex programs with random data. Information and Inference: A Journal of the IMA **3**(3), 224–294 (2014). https://doi.org/10.1093/imaiai/iau005
2. Basar, E.: Index modulation techniques for 5G wireless networks. IEEE Communications Magazine **54**(7), 168–175 (2016). https://doi.org/10.1109/MCOM.2016.7509396
3. Basar, E., Aygolu, Y., Panayırcı, E., Poor, H.V.: Orthogonal frequency division multiplexing with index modulation. IEEE Transactions on Signal Processing **61**(22), 5536–5549 (2013). https://doi.org/10.1109/TSP.2013.2279771
4. Baxter, W., Aboutanios, E., Hassanien, A.: Dual-function MIMO radar-communications via frequency-hopping code selection. In: 2018 52nd Asilomar Conference on Signals, Systems, and Computers, pp. 1126–1130 (2018). https://doi.org/10.1109/ACSSC.2018.8645212
5. Baxter, W., Aboutanios, E., Hassanien, A.: Joint radar and communications for frequency-hopped MIMO systems. IEEE Transactions on Signal Processing **70**, 729–742 (2022). https://doi.org/10.1109/TSP.2022.3142909
6. BouDaher, E., Hassanien, A., Aboutanios, E., Amin, M.G.: Towards a dual-function MIMO radar-communication system. In: 2016 IEEE Radar Conference (RadarConf), pp. 1–6 (2016). DOI https://doi.org/10.1109/RADAR.2016.7485316

7. Cheng, X., Zhang, M., Wen, M., Yang, L.: Index modulation for 5G: Striving to do more with less. IEEE Wireless Communications **25**(2), 126–132 (2018). DOI https://doi.org/10.1109/MWC.2018.1600355
8. Chi, Y., Ferreira Da Costa, M.: Harnessing sparsity over the continuum: Atomic norm minimization for superresolution. IEEE Signal Processing Magazine **37**(2), 39–57 (2020). DOI https://doi.org/10.1109/MSP.2019.2962209
9. Datta, T., Eshwaraiah, H.S., Chockalingam, A.: Generalized space-and-frequency index modulation. IEEE Transactions on Vehicular Technology **65**(7), 4911–4924 (2016). DOI https://doi.org/10.1109/TVT.2015.2451095
10. De Maio, A., Eldar, Y.C., Haimovich, A.M.: Compressed sensing in radar signal processing. Cambridge University Press (2019)
11. Donoho, D.L.: High-dimensional centrally symmetric polytopes with neighborliness proportional to dimension. Discrete & Computational Geometry **35**(4), 617–652 (2006)
12. Doğan Tusha, S., Tusha, A., Basar, E., Arslan, H.: Multidimensional index modulation for 5G and beyond wireless networks. Proceedings of the IEEE **109**(2), 170–199 (2021). DOI https://doi.org/10.1109/JPROC.2020.3040589
13. Eldar, Y.C., Kutyniok, G.: Compressed sensing: theory and applications. Cambridge university press (2012)
14. Foucart, S., Rauhut, H.: Sparse recovery with random matrices. In: A Mathematical Introduction to Compressive Sensing, pp. 271–310. Springer (2013)
15. Fu, R., Liu, Y., Huang, T., Eldar, Y.C.: Structured LISTA for multidimensional harmonic retrieval. IEEE Transactions on Signal Processing pp. 1–1 (2021). DOI https://doi.org/10.1109/TSP.2021.3086593
16. Hassanien, A., Aboutanios, E., Amin, M.G., Fabrizio, G.A.: A dual-function MIMO radar-communication system via waveform permutation. Digital Signal Processing **83**, 118–128 (2018)
17. Huang, T., Liu, Y., Xu, X., Eldar, Y.C., Wang, X.: Analysis of frequency agile radar via compressed sensing. IEEE Transactions on Signal Processing **66**(23), 6228–6240 (2018). DOI https://doi.org/10.1109/TSP.2018.2876301
18. Huang, T., Shlezinger, N., Xu, X., Liu, Y., Eldar, Y.C.: MAJoRCom: A dual-function radar communication system using index modulation. IEEE Transactions on Signal Processing **68**, 3423–3438 (2020). DOI https://doi.org/10.1109/TSP.2020.2994394
19. Huang, T., Shlezinger, N., Xu, X., Ma, D., Liu, Y., Eldar, Y.C.: Multi-carrier agile phased array radar. IEEE Transactions on Signal Processing **68**, 5706–5721 (2020). DOI https://doi.org/10.1109/TSP.2020.3026186
20. Kaddoum, G., Nijsure, Y., Tran, H.: Generalized code index modulation technique for high-data-rate communication systems. IEEE Transactions on Vehicular Technology **65**(9), 7000–7009 (2016). DOI https://doi.org/10.1109/TVT.2015.2498040
21. Kay, S.M.: Fundamentals of statistical signal processing, Volume I: estimation theory. Prentice Hall PTR (1993)
22. Li, Y., Huang, T., Xu, X., Liu, Y., Wang, L., Eldar, Y.C.: Phase transitions in frequency agile radar using compressed sensing. IEEE Transactions on Signal Processing **69**, 4801–4818 (2021). DOI https://doi.org/10.1109/TSP.2021.3099629
23. Ma, D., Huang, T., Liu, Y., Wang, X.: A novel joint radar and communication system based on randomized partition of antenna array. In: 2018 IEEE International Conference on Acoustics, Speech and Signal Processing (ICASSP), pp. 3335–3339 (2018). DOI https://doi.org/10.1109/ICASSP.2018.8462475
24. Ma, D., Huang, T., Shlezinger, N., Liu, Y., Wang, X., Eldar, Y.C.: A DFRC system based on multi-carrier agile FMCW MIMO radar for vehicular applications. In: 2020 IEEE International Conference on Communications Workshops (ICC Workshops), pp. 1–7 (2020). DOI https://doi.org/10.1109/ICCWorkshops49005.2020.9145355
25. Ma, D., Shlezinger, N., Huang, T., Liu, Y., Eldar, Y.C.: Joint radar-communication strategies for autonomous vehicles: Combining two key automotive technologies. IEEE Signal Processing Magazine **37**(4), 85–97 (2020). DOI https://doi.org/10.1109/MSP.2020.2983832

26. Ma, D., Shlezinger, N., Huang, T., Liu, Y., Eldar, Y.C.: Bit constrained communication receivers in joint radar communications systems. In: 2021 IEEE International Conference on Acoustics, Speech and Signal Processing (ICASSP), pp. 8243–8247 (2021). DOI https://doi.org/10.1109/ICASSP39728.2021.9413979
27. Ma, D., Shlezinger, N., Huang, T., Liu, Y., Eldar, Y.C.: FRaC: FMCW-based joint radar-communications system via index modulation. IEEE Journal of Selected Topics in Signal Processing **15**(6), 1348–1364 (2021). DOI https://doi.org/10.1109/JSTSP.2021.3118219
28. Ma, D., Shlezinger, N., Huang, T., Shavit, Y., Namer, M., Liu, Y., C. Eldar, Y.: Spatial modulation for joint radar-communications systems: Design, analysis, and hardware prototype. IEEE Transactions on Vehicular Technology **70**(3), 2283–2298 (2021). DOI https://doi.org/10.1109/TVT.2021.3056408
29. Mao, T., Wang, Q., Wang, Z., Chen, S.: Novel index modulation techniques: A survey. IEEE Communications Surveys & Tutorials **21**(1), 315–348 (2019). DOI https://doi.org/10.1109/COMST.2018.2858567
30. Papoulis, A., Pillai, S.U.: Probability, random variables, and stochastic processes. Tata McGraw-Hill Education (2002)
31. Richards, M.A.: Fundamentals of radar signal processing, 2nd edn. McGraw-Hill Education (2014)
32. Shlezinger, N., Whang, J., Eldar, Y.C., Dimakis, A.G.: Model-based deep learning. arXiv preprint arXiv:2012.08405 (2020)
33. Skolnik, M.I.: Introduction to radar systems, third edition. New York, McGraw Hill Book Co. (2001)
34. Wang, J., Jia, S., Song, J.: Generalised spatial modulation system with multiple active transmit antennas and low complexity detection scheme. IEEE Transactions on Wireless Communications **11**(4), 1605–1615 (2012). DOI https://doi.org/10.1109/TWC.2012.030512.111635
35. Wang, X., Hassanien, A., Amin, M.G.: Dual-function MIMO radar communications system design via sparse array optimization. IEEE Transactions on Aerospace and Electronic Systems **55**(3), 1213–1226 (2019). DOI https://doi.org/10.1109/TAES.2018.2866038
36. Wang, X., Xu, J.: Co-design of joint radar and communications systems utilizing frequency hopping code diversity. In: 2019 IEEE Radar Conference (RadarConf), pp. 1–6 (2019). DOI https://doi.org/10.1109/RADAR.2019.8835576
37. Wehner Donald, R.: High resolution radar. Artech House (1995)
38. Wu, K., Zhang, J.A., Huang, X., Guo, Y.J.: Frequency-hopping MIMO radar-based communications: An overview. IEEE Aerospace and Electronic Systems Magazine **37**(4), 42–54 (2022). DOI https://doi.org/10.1109/MAES.2021.3081176
39. Wu, K., Zhang, J.A., Huang, X., Guo, Y.J., Heath, R.W.: Waveform design and accurate channel estimation for frequency-hopping mimo radar-based communications. IEEE Transactions on Communications **69**(2), 1244–1258 (2021). DOI https://doi.org/10.1109/TCOMM.2020.3034357
40. Wu, K., Zhang, J.A., Huang, X., Guo, Y.J., Yuan, J.: Reliable frequency-hopping mimo radar-based communications with multi-antenna receiver. IEEE Transactions on Communications **69**(8), 5502–5513 (2021). DOI https://doi.org/10.1109/TCOMM.2021.3079270
41. Xu, Z., Petropulu, A., Sun, S.: A joint design of MIMO-OFDM dual-function radar communication system using generalized spatial modulation. In: 2020 IEEE Radar Conference (RadarConf20), pp. 1–6 (2020). DOI https://doi.org/10.1109/RadarConf2043947.2020.9266486
42. Younis, A., Mesleh, R.: Information-theoretic treatment of space modulation MIMO systems. IEEE Transactions on Vehicular Technology **67**(8), 6960–6969 (2018). DOI https://doi.org/10.1109/TVT.2018.2821684
43. Younis, A., Serafimovski, N., Mesleh, R., Haas, H.: Generalised spatial modulation. In: 2010 Conference Record of the Forty Fourth Asilomar Conference on Signals, Systems and Computers, pp. 1498–1502 (2010). DOI https://doi.org/10.1109/ACSSC.2010.5757786